



Microbialites diversity from the Ediacaran of the Anti-Atlas (Morocco): A snapshot of microbial oases thriving in an alkaline volcanic lake

Ibtissam Chraiki, El Hafid Bouougri, Abderrazak El Albani

► To cite this version:

Ibtissam Chraiki, El Hafid Bouougri, Abderrazak El Albani. Microbialites diversity from the Ediacaran of the Anti-Atlas (Morocco): A snapshot of microbial oases thriving in an alkaline volcanic lake. Annales de Paléontologie, 2022, 108 (4), pp.102584. 10.1016/j.annpal.2022.102584 . hal-04520828

HAL Id: hal-04520828

<https://hal.science/hal-04520828>

Submitted on 26 Mar 2024

HAL is a multi-disciplinary open access archive for the deposit and dissemination of scientific research documents, whether they are published or not. The documents may come from teaching and research institutions in France or abroad, or from public or private research centers.

L'archive ouverte pluridisciplinaire **HAL**, est destinée au dépôt et à la diffusion de documents scientifiques de niveau recherche, publiés ou non, émanant des établissements d'enseignement et de recherche français ou étrangers, des laboratoires publics ou privés.

Microbialites diversity from the Ediacaran of the Anti-Atlas-Morocco: A snapshot of microbial oases thriving in an alkaline volcanic lake

La diversité des microbialites Ediacariennes de l'Anti-Atlas-Maroc : Un aperçu des oasis microbiennes prospérant dans un lac volcanique alcalin

Ibtissam Chraiki¹, El Hafid Bouougri¹, Abderrazak El Albani^{2*}

¹Department of Geology, Faculty of Sciences-Semlalia, Cadi Ayyad University, POBox2390, My Abdellah Str., 40000 Marrakesh, Morocco.

²University of Poitiers, UMR-CNRS IC2MP 7285, Poitiers, France.

* Corresponding author: abder.albani@univ-poitiers.fr

Authors mail:

Ibtissamchraiki@gmail.com

bouougri@uca.ma

ABSTRACT

The Moroccan Anti-Atlas belt preserves an exceptional record of an Ediacaran microbial biosphere. The Amane Tazgart Formation of the Ouarzazate Group corresponds to an Ediacaran volcanic alkaline lake depositional system (ca. 571 Ma) where microbial buildups accreted in an extreme environment. These microbial accumulations are exceptional not only for their diverse range of extreme conditions but also for their significance in understanding the early biosphere and earth's habitability. A description of these buildups provides insights into their Spatio-temporal distribution. The lower part consists of thrombolitic limestones, usually displaying irregular to patchy mesoclot, associated with composite and stromatolitic

buildups. The upper part dominated by clastic stromatolites exhibits a variety of morphotypes ranging vertically from planar wrinkly laminated to large domes. The transitional morphotypes are made of linked and vertically oriented or inclined columns, grading upward to cone-shaped domes. The increase in laminated fabrics and the decrease in clotted fabrics toward the top of the section indicate that environmental conditions were likely suitable for coexisting both fabrics during microbial carbonate accretion. The demise of carbonate production at the late stage coincides with riverine input of clastic sediments, subsequently followed during low sediment input by growth of siliciclastic stromatolites.

Keywords : Extreme environment, stromatolites, thrombolites, composite microbialites, Ediacaran, Anti-Atlas

RESUME

La chaîne de l'Anti-Atlas marocain conserve un témoignage exceptionnel d'une biosphère microbienne d'âge édiacarien. La formation d'Amane Tazgart du groupe de Ouarzazate correspond à un système de dépôt lacustre alcalin volcanique de l'Édiacarien (vers 571 Ma) où des accumulations microbiennes se sont accrétées dans un environnement extrême. Ces dernières sont exceptionnelles à la fois pour leur diversité dans des conditions extrêmes, mais aussi pour leur apport dans la compréhension de la biosphère primitive et de l'habitabilité de la Terre à cette époque. Une description précise de ces accumulations donne un aperçu de leur distribution spatio-temporelle. La partie inférieure est constituée de calcaires thrombolitiques, présentant généralement des mésoclots irréguliers ou parcellaires, associés à des accumulations composites et stromatolitiques. La partie supérieure dominée par des stromatolites clastiques présente une variété de morphotypes allant verticalement de stromatolites horizontales et ondulés à de grands dômes. Les morphotypes transitoires sont constitués de colonnes liées et orientées verticalement ou inclinées, progressant vers le haut pour former des dômes coniques. L'augmentation des tissus laminés et la diminution des tissus coagulés vers le haut de la section indiquent que les conditions environnementales étaient probablement adaptées à la coexistence des deux types de fabriques pendant l'accrétion microbienne des carbonates. La baisse de la production de carbonate au stade tardif coïncide avec l'apport fluvial de sédiments clastiques, suivi ultérieurement, pendant un faible apport de sédiments, par la croissance de stromatolites siliciclastiques.

Mots clés : Environnement extrême, stromatolites, thrombolites, microbialites composites, Ediacarien, Anti-Atlas

1. Introduction

Microbialites, microbially-related products, and fossilized remains are the main components of the early earth's biosphere that appeared since ~3.7 Ga (e.g. Allwood et al., 2006; Dodd et al., 2017; Hickman-Lewis et al., 2018; Homann et al., 2018). The oldest biosignatures and life's evidence were recorded in the Archean and Proterozoic times and known from environmental settings ranging from terrestrial volcanic-related hydrothermal seeps and alkaline lakes, all indicative of extreme conditions (e.g. Sugitani et al., 2015; Westall et al., 2015; Djokic et al., 2017; Lepot, 2020). Among others, the main diagnostic features for the biogenicity of organo-sedimentary deposits include fossil remnants like calcimicrobes and fossilized cells, textures and microfabrics typical of bio-accretionary processes. In the rock records, the biotic-derived products and biosignatures can be constrained at various scales, from rock samples to chemical elements and molecular remains (e.g., calcimicrobes and biomarkers). Eventually, at the field and microscopic scales, the biotic origin is mainly based on recognizing typical macroscale and mesoscale morphotypes, together with evidence of microfabrics and textures indicatives of microbially-related processes (e.g. Gerdes, 2007; Riding, 2011).

Volcanic alkaline lakes are among the terrestrial settings where microbial communities flourish (Pecoraino et al., 2015). Modern examples provide significant insights into the environmental and ecological parameters and the interplay of biotic and abiotic processes within deposited sediment and mineral products (e.g. Cangemi et al., 2016; Chacón B. et al., 2018; Kaźmierczak et al., 2011). As a restricted-basin systems, volcanic lakes and their microbial communities are very sensitive to intrinsic and extrinsic parameters such as water chemistry and alkalinity, available nutrients, hydrothermal and riverine inputs, climate changes, and lake-level water fluctuations. Such parameters can be constrained from the stacking patterns of sediments as well as from geochemical proxies of sediments mainly of carbonate origin. Microbial communities are sensitive to such parameters, and microbialites are useful for understanding the biotope features as they preserve signatures of several parameters during the bio-sedimentary accretion and early diagenesis.

Microbialites *sensu* Burne and Moore, (1987) represented by-a wide variety of morphotypes at the macroscale ranging from flat-laminated to domal and from patchy small bioherms to thick and widespread bioherms and reefs. In contrast to siliciclastic microbialites, which are

exclusively laminated (e.g. Gerdes, 2007; Porada and Bouougri, 2007; Bouougri and Porada, 2011; Homann et al., 2015), microbial carbonates produce a variety of textures and fabrics, including well-laminated (i.e. stromatolites and dendrolites) and non-laminated (i.e. Thrombolites, Leiolites), (e.g. Riding, 2011). Throughout the geological record and modern depositional settings, carbonate microbialites occur in a broad spectrum of environments ranging from shallow marginal areas to deep water settings in aquatic lacustrine and marine settings. In contrast, clastic microbialites appear restricted to shallow marginal settings with quiet physical conditions. The siliciclastic microbialites have a common genetic process with agglutinated sandy-carbonate microbialites, consisting mainly of trapping and binding clastic and carbonate particles within the mat fabric (Reid et al., 2000; Gerdes, 2007). However, considering the geological record and occurrences from modern settings, the morphotype diversity in siliciclastic microbialites is low and appears limited to planar and low-relief domal biolaminites (Gerdes, 2007; Bouougri and Porada, 2011).

This paper aims to present an example of a geologic record of microbial oases flourishing in extreme environments, likely similar to some of the early earth and where microbial bio-sedimentary accretion processes produced a variety of microbial deposits. Within this Ediacaran volcanic lake, microbial communities interacting with sediments and depositional settings develop a variety of morphotypes and fabrics in both carbonate- and clastic-dominated sedimentation. The biotic macro- and microstructures can be recognized at various scales in both deposits. The clastic microbialites preserve a variety of morphotypes with a typical stacking pattern. The studied example here provides a window to the ecological diversity in volcanic alkali lakes and to understanding microbial adaptation to depositional settings and thus may serve for comparing with early earth's biosphere.

2. Geological setting

The southern Moroccan Anti-Atlas belt stretches ENE-WSW for more than 600 kilometers, from the Atlantic margin in west Africa to the Tafilalt plain in southern Morocco ([Fig. 1A](#)). The Eburnean Paleoproterozoic and Pan-African Neoproterozoic basement is unconformably overlain by an Upper Ediacaran and Paleozoic succession that includes the thick volcanic and volcanoclastic Ouarzazate Supergroup (Thomas et al., 2002). The Ouarzazate supergroup was previously subdivided into two main sections separated by an angular unconformity: (i) a lower section (labeled XIIIm) named as Mançour Group, basically composed of rhyolitic to andesitic

volcanic rocks, volcanic breccia, conglomerate, and volcaniclastic rocks, and (ii) an upper section (labeled XIIIIs) named as Imlas Group, containing rhyolitic flows interbedded with volcaniclastic rocks (Thomas et al., 2004; Tuduri et al., 2018; Walsh et al., 2012). The majority of the volcanic rocks are peraluminous to metaluminous, with lithologies spanning from andesitic basalts to rhyolitic lithologies with high-K calc-alkaline to shoshonitic affinities (Walsh et al., 2012). The structural, sedimentological, and volcanic features indicate subaerial effusive volcanic activity from several active centers containing calderas, and subaerial sedimentary sequences of alluvial, fluvial, and colluvial origin. The Ediacaran Oued Dar'a caldera, on which this paper is focused, is large rectangular-shaped volcanic structure 11 km wide and 18 km long in the lower Ouarzazate Supergroup to the southeast of the Saghro massif ([Fig. 1A, B](#)). The caldera, which is located along a northeast corridor, is made up of a remarkably well-preserved infill of trachytic, trachydacitic, and rhyolitic ash-flow tuffs ponded within a large volcano (Walsh et al., 2012). Pink granite, interpreted as the parent magma of the volcanic rocks, intrudes the northeast margin ([Fig. 1B](#)). The southwestern margin (Choubert & Faure-Muret, 1970) is characterized by a 200 m coarse-grained, quartz-rich, and granulated volcaniclastic deposit resting on the caldera's infill ash-flow tuff and intercalated with purplish-green microbialites (Álvaro et al., 2010; Álvaro & González-Acebrón, 2019; Walsh et al., 2012). According to Walsh et al., (2012), the age of the caldera infill is estimated to be 571.5 Ma, the age of the last major volcanic eruption from the caldera ([Fig. 1B](#)).

This research focuses on a decametre-scale lacustrine deposit characterized by microbialite bearing, known as Amane Tazgart (Harrison et al., 2008; Chraiki et al., 2020), and as Amane N'Tourhart (Álvaro et al., 2010; Álvaro and González-Acebrón, 2018; Choubert., 1952). The Amane Tazgart deposits are situated on the western edge of the Saghro inlier ([Fig. 1B](#)), approximately 25 kilometers southeast of the Ouarzazate classical geological field trip stops along the Ouarzazate-Zagora Agdz road (e.g., Choubert., and Faure-Muret, 1970). Given their limited geographic expansion and the apparent closeness of domal and conical stromatolites, Choubert and Faure-Muret (1970) were the first to propose a lacustrine depositional setting for these meter-thick, carbonate-bearing volcano-sedimentary units. The Amane Tazgart microbialites were primarily controlled by the caldera's volcanic and geothermal activity, in combination with silicate hydrolysis under subtropical conditions (Álvaro and González-Acebrón, 2018; Chraiki et al., 2020).

3. Methodology

This study describes the diversity from an Ediacaran example of microbialites, thriving in an extreme environment of an alkaline volcanic lake. Microbialites were examined at various scales including detailed field surveys, polished slabs, and thin sections. Logging, sampling, and facies analysis were carried out along transects cutting the whole succession and 49 samples were collected for petrographic and textural studies. At the University of Poitiers, thin sections were studied for detailed mineralogy using a ZEISS Discovery V8 microscope equipped with an AxioCamERc 5s camera. Raman Spectra were performed on non-covered thin sections for documenting the mineralogical nature of dark laminae within stromatolites. The Raman spectra were obtained with a HORIBA JOBIN YVON Labram HR800UV, an integrated Olympus confocal microscope connected to a CCD detector using a Peltier-cooled charge at the University of Poitiers. All analyses were performed employing a 632 nm Ar+ laser of 0,05 mW, 200 µm confocal hole, 600 grooves/mm grating, and 5 mm spatial resolution. LabSpec 5 software was used for data recording and treatment.

4. Results

4.1. *Microbialite diversity*

The Amane Tazgart succession is up to ~15m thick and can be subdivided into two distinct lithologic parts, lower carbonate-dominated and upper clastic-dominated deposits. Both parts preserve several morphotypes of microbialites and are associated with carbonate and clastic non-biogenic deposits (Chraiki et al., 2020). Microbialite facies appear on top of meter-thick cycles often starting with a clastic layer forming lenses of micro-conglomerates and current rippled and thinly bedded sandstone. Carbonates and siliciclastic microbialites preserve at the macroscale and mesoscale a variety of typical biogenic structures, however, the diversity in siliciclastic microbialites appears unusual compared to the geologic record for this kind of organo-sedimentary products (e.g. Gerdes and Krumbein, 1987; Gerdes et al., 2000; Druschke et al., 2009; Bouougri and Porada, 2011) .

4.2. *The carbonate microbialites*

Several morphotypes and textures within the carbonate microbialites were identified, varying from thrombolites to stromatolites and composite microbialites. Thrombolites were observed mainly within the lower part of the section, forming isolated patches or coalescent meter-tick

domes ([Fig. 2, 3A, B](#)). They are characterized by irregular to patchy carbonate mesoclot surrounded by cements or fine-grained epiclastic matrix ([Fig. 3C](#)). Toward the middle part and top of the section, the abundance of stromatolitic fabric becomes more abundant. In some bioherms, both clotted and laminated fabrics occur together forming thus composite meter-thick coalescent dome features ([Figs. 3B, 3D](#)). Such fabrics were observed at different scales, ranging from the macro- to micro-scales. Flat large domal stromatolites consist of laterally linked domes forming beds up to 30 cm thick with domes ranging from 30cm to 1 m in diameter ([Fig. 3E](#)). In the upper part of the section; stromatolitic fabrics are more abundant with microbial beds displaying columnar and domal morphotypes ([Fig. 3F, 4](#)). On top of carbonate microbialites, a layer with planar stromatolites up to 30 cm thick, preserves on the bed surface a wide polygonal network of upturned margins ([Fig. 3G](#)). The upturned margins are up to 6 cm thick and demarcate irregular polygons up to 50 cm in length and 40 cm in width. A secondary irregular polygonal generation is well-developed inside the main polygons ([Fig. 3H](#)).

4.3. The epiclastic microbialites

Epiclastic microbialites constitute the last stromatolitic bed of Amane Tazgart succession and is separated from the carbonate-dominated lower part by a meter-thick siliciclastic layer dominated by thin to medium bedded sandstone that preserves current and oscillation ripples on bedding surfaces. These microbialites form a single bed up to 2 meters thick bounded on top by thick peperites ([Fig. 5](#)) (Chraiki et al., 2020). Various morphotypes can be recognized and arranged from bottom to top into a succession showing an increase in the size and the relief of the stromatolites ([Fig. 5](#)). The bed starts with planar wrinkly laminated to pseudo-columnar stromatolites ([Fig. 6A](#)), grading upward to laterally linked columnar-hemispherical stromatolites ([Fig. 6B, 6C](#)). The columns are up to 40 cm high and 8 cm wide ([Fig. 6C](#)), and they appear often inclined with NW-SE general trend ([Fig. 6B](#)). Toward the top of the stromatolitic bed, the columnar forms are replaced by wide domes with width up to 20cm ([Fig. 6D](#)). They form dome-shaped and cone-shaped domes with very narrow interdomes space. The Uppermost part consists of large domes up to 0.5 m high and 40 cm in width ([Fig. 6E](#)), and to conical morphotypes reaching heights of 0.1 m and varied widths of 0.1-0.2 m ([Fig. 6F](#)). The head of the large domes can be simple or composite with several medium-scale domes forming a bunch ([Fig. 6G](#)). Within the composite head, various sizes of domes are observed ([Fig. 6G](#)). In the section exposed along the river of Amane cutting the succession

(Fig. 5), the large domes are separated by interdomes deposited showing an alternation of continuous stromatolitic layers and epiclastic interbeds pinching toward the head of the dome (Fig. 6H, 6I).

4.4. Microfabric: Carbonate vs clastic microbialites

The microfabric textures of Amane Tazgart microbialites show a wide diversity which can be observed at the scale of the same morphotype. Within the thrombolitic fabric (Fig. 4A), mesoclotls vary widely in shape and size ranging from 3 mm to 5 centimeters. They are isolated and sometimes connected in different shapes. They comprise a core surrounded by an outer layer (Fig. 7A, 7B). The core is made up of clotted to peloidal micrite, with scattered sand- to silt-sized clastic grains (Fig. 7A, 7B). The outer layer consists of fibrous to botryoidal calcite (Fig. 7B). Voids between mesoclotls are usually filled with a matrix of sand- to silt-sized clastic sediments or drusy calcite (Fig. 4A, 7B).

The matrix is partially silicified and occasionally preserves a wavy and wrinkly lamination made of thin dark crusts and clastic laminae (Fig. 7A, 7B). Composite microbialites consist of patches of mesoclotls similar to those of thrombolites, overlain and draped by a laminated fabric with alternating dark micritic and white microsparitic laminae (Fig. 4B, 4D, 7D). Flat large domal stromatolites preserve texture typical of tufted microbial mats (Fig. 7E), alternating with dark micritic to microsparitic laminae (Fig. 7E). The last stromatolitic facies of carbonate succession (Fig. 4E), correspond to alternating of dark fine-grained micritic, microsparitic laminae, and sand-sized clastic laminae (Fig. 7F). The microfabric of polygonal stromatolites is similar to that of carbonate stromatolite.

Epiclastic stromatolites display a wide variety of laminae compared to carbonate stromatolites (Fig. 4F-G): fine-grained micritic laminae, coarse-grained agglutinated laminae, spary crust, iron-rich laminae, and iron crust. Flat laminated (Fig. 4F) and columnar stromatolites (Fig. 4G) are characterized by an alternation of fine-grained micritic laminae and fine-grained or coarse-grained wrinkled mats with trapped silt and sand-sized grains (Fig. 7G). Domal and conical stromatolites are made up of an alternation of coarse-grained wrinkled laminae, spary crusts, iron-rich laminae, and micritic laminae (Fig. 7I, 7J, 7K). The alternation and the association of laminae may differ in the same sample but are generally all associated. Because of the presence of spary crust associated with the different types of microbial laminae, domal

and conical stromatolites can be classified as hybrid crust stromatolites. Several gas domes and gas escape structures were identified within flat domal and columnar stromatolites (Fig. 7H), while tufts were mainly observed in domal and conical stromatolites (Fig. 7I, 7K). The microfabric of flat laminated to pseudo-columnar stromatolites in the interdome space is different from that of flat laminated stromatolites observed at the base of the microbialitic bed. This microfabric consists of an alternation of coarse-grained wrinkled laminae and wrinkled iron-rich laminae bounding isolated silt and sand-sized clastic grains (Fig. 7L). Micritic laminae in epiclastic stromatolite (Fig. 7G, 7K) are more peloidal and darker than those of stromatolitic carbonate (Fig. 7F), and appear as opaque in polarized analyzed light (Fig. 7J). Raman spectroscopy was performed on the different dark laminae (micritic and coarse-grained wrinkled mats) from several samples in order to constrain their nature and diversity and if they preserve any organic carbon remains. The results revealed the presence of hematite in both coarse-grained wrinkled laminae (Fig. 8A, 8B) and micritic laminae (Fig. 8C, 8D), with no evidence for organic carbon preservation.

5. Discussion : The genesis of the Amane Tazgart microbialites

Since the late Neoproterozoic, thrombolites have gradually increased in abundance (Grotzinger, 2000). They are considered a distinct type of microbialite in modern and many Paleozoic examples. The microbialites of Amane Tazgart succession start with the deposition of thrombolitic coalescent domes, of irregular to patchy mesoclot in a shallow lake. The presence of terrigenous sand- to silt-sized particles, embedded in fine-grained microbial micritic mesoclot likely indicates that the mesoclot primarily derived from the trapping and binding of sediment particles by microbial films, associated with carbonate precipitation induced by biochemical processes (Dongjie et al., 2013; Riding, 2011). The sharp contact between nuclei and rims, as well as the distinct components in each, point to distinct formation mechanisms. The nuclei of mesoclot, in particular, were most likely formed by the trapping of detrital particles and the organo-mineralization of microbial cells or colonies and the EPS secreted by them, while the rims fringing the clots constitute cement formed by carbonate precipitation enabled by interactions between microbes and the surrounding environment (Dongjie et al., 2013). Following the classification of Riding, (2011), the studied thrombolites can be classified as coarse agglutinated thrombolites. The nucleation of thrombolites on an irregular surface and locally on lens-shaped conglomerates (Chraiki et al., 2020), indicates a shallow environmental deposition. Polygonal stromatolites are

distinguished primarily by the presence of straight to slightly curved microbial shrinkage cracks, which have often evolved into cracks with upturned margins, resulting in a polygonal pattern (Bouougri and Porada, 2007; Cuadrado et al., 2014; Bouougri and Porada, 2018). These patterns were interpreted to be induced by the interplay of mat shrinkage and growth in the marginal area with periodic subaerial exposure (Bouougri and Porada, 2007; Porada and Druschel, 2010). Modern analogs in tidal flats environment reveal that at low tide, the edges of polygons are upturned and that active growth of new mats in cracks openings overgrows and stabilizes the polygon edges (Bouougri and Porada, 2007).

Although local environmental conditions influenced the relative proportions and distributions of stromatolitic and thrombolitic microbialites, composite microbialites suggest that differences between clotted and laminated microbialites cannot be assigned to a simple change in the depositional environment (Harwood and Sumner, 2011; Chraiki et al., 2020). The coexistence of distinct clotted and laminated textures suggests that they grew in the same setting, and thus environmental conditions alone cannot explain the observed textural variations. The resulting co-occurrence of thrombolitic and stromatolitic textures may be induced by the concurrent growth of morphologically distinct microbial populations (Harwood and Sumner, 2011). Because composite microbialites imply that internal textures reflect community morphology rather than environmental variations, the presence of thrombolitic or stromatolitic domes as separate textures suggest that one community morphology predominates (Harwood and Sumner, 2011). The increase in laminated fabrics and decrease in clotted fabrics toward the top of the section ([Fig. 4](#)) indicates that environmental conditions were likely to be favorable for the coexistence of both thrombolitic and stromatolitic fabrics during carbonate deposition. However, the conditions were later evolved to only allow the existence of microbial populations responsible for stromatolite genesis.

The features and facies described in the Amane Tazgart as well as the overall geodynamic setting point toward a lacustrine setting in which microbial communities thrived under specific conditions (Chraiki et al., 2020). The sedimentary features of microbialitic and non-microbialitic deposits and the vertical stacking pattern of the facies indicate lacustrine cycles with low-energy conditions punctuated by high-energy events. The high-energy stage is associated with erosive currents producing mainly coarse-grained clastic carbonates dominated by microbialitic clasts and cross-bedded calcarenites ([Fig. 9A, 9B](#)). In clastic part

of the shoreline, planar laminated sandstone is dominating with bedding surface displaying symmetric and asymmetric ripples (Fig. 9C, 9D). These clastic deposits were interpreted to be generated and deposited in the margins of the lake (Fig. 10A). Whereas, the low-energy conditions, that generally occurred in the central part of the lake, were favorable for microbial mats development, producing different types of carbonate and clastic microbialites (Fig. 10B). The subdivision of the Amane Tazgart succession into lower carbonates and upper clastic parts may imply significant chemical change and clastic sediment supply to the lake (Chraiki et al., 2020). The transition from calcite-dominated to quartz-dominated deposits indicates a decrease in calcium carbonate saturation from the bottom to the top of the succession. The iron enrichment of micritic laminae and the abundance of hematite wrinkly laminae in clastic stromatolites compared to carbonate microbialites may be attributed to the lake's chemistry, which likely changed from a carbonate-saturated to an iron and silica-saturated lake. This saturation required a sustained source of iron to precipitate consistently hematite laminae, taking into account the paleoenvironmental position of the lake in a caldera setting, the source of iron was likely delivered through hydrothermal activity (Hiatt et al., 2020).

6. Conclusion

The Ediacaran Amane succession in the Anti-Atlas belt provides an example of microbial communities thriving in a volcanic setting. By considering features at meso- and micro-scale, various types of microbialites were recognized in both carbonate and siliciclastic biolithites. The framework and diversity in carbonate microbialites appear similar to that of modern examples with the co-occurrence of clotted and laminated fabrics typical of thrombolites and stromatolites, whereas the diversity in siliciclastic microbialites appear unusual and various morphotypes were identified. The available sediments as well as the chemistry of the lake together with other parameters may have controlled this diversity and may need more featured studies. However and considering the vertical trend, the significant clastic input at the late stage of the lake induced a drastic shift from carbonate-bounding to clastic-bounding in the microbialites.

Acknowledgments

This work was supported and carried out under the Scientific project funded by Hassan II Academy of Sciences and Technology-Morocco (Project Leader, Prof. El Albani) and the

PhD work of I.C. Support was also provided by “La Région Nouvelle Aquitaine” and by the Faculty of Sciences Semlalia of Marrakech. We would like to thank the reviewers for their critical review and comments that greatly improved the manuscript, and the editorial board for the prompt editing of this paper. We also like to thank Nadia Guignard, Claude Fontaine, Claude Laforest and Celine Boissard from the University of Poitiers for technical assistance.

References

- Allwood, A.C., Walter, M.R., Kamber, B.S., Marshall, C.P., Burch, I.W., 2006. Stromatolite reef from the Early Archaean era of Australia. *Nature* 2006 4417094 441, 714–718. <https://doi.org/10.1038/nature04764>
- Álvaro, J.J., Ezzouhairi, H., Ayad, N.A., Charif, A., Solá, R., Ribeiro, M.L., 2010. Alkaline lake systems with stromatolitic shorelines in the Ediacaran volcanosedimentary Ouarzazate Supergroup, Anti-Atlas, Morocco. *Precambrian Research* <https://doi.org/10.1016/j.precamres.2010.02.009>
- Álvaro, J.J., González-Acebrón, L., 2018. Sublacustrine hydrothermal seeps and silicification of microbial bioherms in the Ediacaran Oued Dar'a caldera, Anti-Atlas, Morocco. *Sedimentology sed.12568.* <https://doi.org/10.1111/sed.12568>
- Bouougri, E.H., Porada, H., 2007. Complex structures associated with siliciclastic biolaminites. In: Schieber et al., (Eds.), *An Atlas of microbial mat features preserved within the siliciclastic rock record*, Elsevier, Amsterdam, pp.111-115.
- Bouougri, E.H., Porada, H., 2018. Diagnostic features for interplay of microbial mats shrinkage and growth: An actualistic approach for biosignatures in rock record and Earth's early biosphere. In: Geobonn, Bonn Germany, pp. 10.
- Bouougri, E.H., Porada, H., 2011. Biolaminated siliciclastic deposits. *Lect. Notes Earth Sciences* 131, 507–524. https://doi.org/10.1007/978-3-642-10415-2_30
- Burne, R.V., Moore, L.S., 1987. Microbialites: Organosedimentary Deposits of Benthic Microbial Communities. *Palaeos* 2, 241. <https://doi.org/10.2307/3514674>
- Cangemi, M., Censi, P., Reimer, A., D'Alessandro, W., Hause-Reitner, D., Madonia, P., Oliveri, Y., Pecoraino, G., Reitner, J., 2016. Carbonate precipitation in the alkaline lake Specchio di Venere (Pantelleria Island, Italy) and the possible role of microbial mats. *Applied Geochemistry* 67, 168–176. <https://doi.org/10.1016/j.apgeochem.2016.02.012>
- Chacón B., E., Aranda-Gómez, J.J., Charles-Polo, M., Sánchez-Ramos, M.A., Rivera-Muñoz, E.M., Levresse, G., Millán-Malo, B., 2018. Biothermal thrombolites of the crater lake Rincón de Parangeo in Central México. *Journal of South American Earth Sciences* 85, 236–249. <https://doi.org/10.1016/j.jsames.2018.04.013>
- Choubert, G., Faure-Muret, A., 1970. Les corrélations du Précambrien, Anti-Atlas occidental et central. Colloque international sur les corrélations du Précambrien: Agadir – Rabat, 3–23 mai 1970. Livret guide de l'excursion: Anti-Atlas occidental et central. *Notes Mémoires du Service Géologique du Maroc* 229 259.

Choubert G., 1952. Histoire géologique du domaine de l'Anti-Atlas. Notes Mémoires du Service Géologique du Maroc 100 196.

Chraiki, I., Bouougri, E.H., Fru, E.C., Lazreq, N., Youbi, N., Boumehdi, A., Aubineau, J., Fontaine, C., Albani, A. El, 2020. A 571 million-year-old alkaline volcanic lake photosynthesizing microbial community, the Anti-Atlas, Morocco. *Geobiology*. <https://doi.org/10.1111/GBI.12425>

Cuadrado, D.G., Perillo, G.M.E., Vitale, A.J., 2014. Modern microbial mats in siliciclastic tidal flats: Evolution, structure and the role of hydrodynamics. *Marine Geology* 352, 367–380. <https://doi.org/10.1016/j.margeo.2013.10.002>

Djokic, T., VanKranendonk, M.J., Campbell, K.A., Walter, M.R., Ward, C.R., 2017. Earliest signs of life on land preserved in ca. 3.5 Ga hot spring deposits. *Nature Communication* 8, 1–9. <https://doi.org/10.1038/ncomms15263>

Dodd, M.S., Papineau, D., Grenne, T., Slack, J.F., Rittner, M., Pirajno, F., Neil, J.O., Little, C.T.S., 2017. Evidence for early life in Earth's oldest hydrothermal vent precipitates. *Nature Publication Gr.* 543, 60–64. <https://doi.org/10.1038/nature21377>

Dongjie, T., Xiaoying, S., Ganqing, J., Yunpeng, P., Wenhao, Z., Yuan, W., Min, L., 2013. Environment controls on Mesoproterozoic thrombolite morphogenesis: A case study from the North China Platform. *Journal of Palaeogeography* 2, 275–296. <https://doi.org/10.3724/SP.J.1261.2013.00031>

Druschke, P.A., Jiang, G., Anderson, T.B., Hanson, A.D., 2009. Stromatolites in the Late Ordovician Eureka Quartzites: Implications for microbial growth and preservation in siliciclastic setting. *Sedimentology* 56, 1275–1291. doi: 10.1111/j.1365-3091.2008.01033.x

Gerdes, G. and Krumbein, W.E., 1987. Biolaminated Deposits. *Lecture Notes in Earth Sciences* 9, 1–183.

Gerdes, G., Klenke, Th. and Noffke, N., 2000. Microbial signatures in peritidal siliciclastic sediments: a catalogue. *Sedimentology* 47, 279–308.

Gerdes, G., 2007. Structures left by modern microbial mats in their host sediments. In: Schieber, J., Bose, P.K., Eriksson, P.G., Banerjee, S., Sarkar, S., Altermann, W., Catuneanu, O. (Eds.), *Atlas of Microbial Mat Features Preserved within the Siliciclastic Rock Record*. Elsevier, Amsterdam.

Grotzinger, J.P., 2000. Facies and paleoenvironmental setting of Thrombolite-Stromatolite Reefs, Terminal Proterozoic Nama Group (ca. 550–543 Ma), central and southern Namibia. *Communs geol. Surv. Namibia* 12, 251–264.

Harrison, R.W., Yazidi, A., Benziane, F., Quick, J.E., El Fahssi, A., Stone, B.D., Yazidi, M., Saadane, A., Walsh, G.J., Aleinikoff, J.N., Ejjaouani, H. and Kalai, M. (2008) Carte géologique au 1/50 000, Feuille Tizgui. Notes et Mémoires du Service Géologique du Maroc, 470.

Harwood, C.L., Sumner, D.Y., 2011. Microbialites of the Neoproterozoic Beck Spring Dolomite, Southern California. *Sedimentology* 58, 1648–1673. <https://doi.org/10.1111/j.1365-3091.2011.01228.x>

Hiatt, E.E., Pufahl, P.K., Guimarães da Silva, L., 2020. Iron and phosphorus biochemical systems and the Cryogenian-Ediacaran transition, Jacadigo basin, Brazil: Implications for the Neoproterozoic oxygenation event. *Precambrian Res.* 337. <https://doi.org/10.1016/j.precamres.2019.105533>

Hickman-Lewis, K., Cavalazzi, B., Foucher, F., Westall, F., 2018. Most ancient evidence for life in the Barberton greenstone belt: Microbial mats and biofabrics of the \square 3.47 Ga Middle Marker horizon. *Precambrian Research* 312, 45–67. <https://doi.org/10.1016/j.precamres.2018.04.007>

Homann, M., Heubeck, C., Airo, A., Tice, M.M., 2015. Morphological adaptations of 3.22 Ga-old tufted microbial mats to Archean coastal habitats (Moodies Group, Barberton Greenstone Belt, South Africa). *Precambrian Research* 266, 47–64. <https://doi.org/10.1016/j.precamres.2015.04.018>

Homann, M., Sansjofre, P., Van Zuilen, M., Heubeck, C., Gong, J., Killingsworth, B., Foster, I.S., Airo, A., Van Kranendonk, M.J., Ader, M., Lalonde, S. V., 2018. Microbial life and biogeochemical cycling on land 3,220 million years ago. *Nat. Geosci.* 2018 119 11, 665–671. <https://doi.org/10.1038/s41561-018-0190-9>

Kaźmierczak, J., Kempe, S., Kremer, B., López-García, P., Moreira, D., Tavera, R., 2011. Hydrochemistry and microbialites of the alkaline crater lake Alchichica, Mexico. *Facies* 57, 543–570. <https://doi.org/10.1007/s10347-010-0255-8>

Lepot, K., 2020. Signatures of early microbial life from the Archean (4 to 2.5 Ga) eon. *Earth-Science Review* <https://doi.org/10.1016/j.earscirev.2020.103296>

Pecoraino, G., D'Alessandro, W., & Inguaggiato, S. (2015). The other side of the coin: geochemistry of alkaline lakes in volcanic areas. In *Volcanic lakes* (pp. 219-237). Springer, Berlin, Heidelberg. <https://doi.org/10.1007/978-3-642-36833-2>

Porada, H., Druschel, G., 2010. Evidence for participation of microbial mats in the deposition of the siliciclastic “ore formation” in the Copperbelt of Zambia. *Journal of African Earth Sciences* 58, 427–444. <https://doi.org/10.1016/J.JAFREARSCI.2010.04.006>

Reid, R.P., Visscher, P.T., Decho, A.W., Stoltz, J.F., Bebout, B.M., Dupraz, C., Macintyre, I.G., Paerl, H.W., Pinckney, J.L., Prufert-Bedout, L., Steppe, T.F., DesMarais, D.J., 2000. The role of microbes in accretion, lamination and early lithification of modern marine stromatolites. *Nature* 406, 989-992. doi: 10.1038/35023158

Riding, R., 2011. Microbialites, stromatolites, and thrombolites. *Encyclopedia of Earth Sciences Series*, Springer, pp. 635-654. <https://doi.org/10.1007/978-1-4020-9212-1>

Sugitani, K., Mimura, K., Takeuchi, M., Yamaguchi, T., Senda, R., Asahara, Y., Wallis, S., Van Kranendonk, M.J., 2015. A Paleoarchean coastal hydrothermal field inhabited by diverse microbial communities: the Strelley Pool Formation, Pilbara Craton, Western Australia. *Geobiology* 13, 522-545. <https://doi.org/10.1111/gbi.12150>

Thomas, R.J., Chevallier, L.P., Gresse, P.G., Harmer, R.E., Eglington, B.M., Armstrong, R.A., De Beer, C.H., Martini, J.E.J., De Kock, G.S., Macey, P.H., Ingram, B.A., 2002. Precambrian evolution of the Sirwa Window, Anti-Atlas Orogen, Morocco. *Precambrian Research* 118, 1–57. [https://doi.org/10.1016/S0301-9268\(02\)00075-X](https://doi.org/10.1016/S0301-9268(02)00075-X)

Thomas, R.J., Fekkak, A., Ennih, N., Errami, E., Loughlin, S.C., 2004. A new lithostratigraphic framework for the Anti-Atlas Orogen, Morocco. *Journal of African Earth Sciences* 39, 217–226. <https://doi.org/10.1016/j.jafrearsci.2004.07.046>

Tuduri, J., Chauvet, A., Barbanson, L., Bourdier, J.L., Labriki, M., Ennaciri, A., Badra, L., Dubois, M., Ennaciri-Leloix, C., Sizaret, S., Maacha, L., 2018. The Jbel Saghro Au(-Ag, Cu) and Ag-Hg metallogenetic province: product of a long-lived ediacaran tectono-magmatic evolution in the moroccan Anti-Atlas. *Minerals* 8. <https://doi.org/10.3390/min8120592>

Walsh, G.J., Benziane, F., Aleinikoff, J.N., Harrison, R.W., Yazidi, A., Burton, W.C., Quick, J.E., Saadane, A., 2012. Neoproterozoic tectonic evolution of the Jebel Saghro and Bou Azzer—El Graara inliers, eastern and central Anti-Atlas, Morocco. *Precambrian Research* 216–219, 23–62. <https://doi.org/10.1016/J.PRECAMRES.2012.06.010>

Westall, F., Campbell, K.A., Bréhéret, J.G., Foucher, F., Gautret, P., Hubert, A., Sorieul, S., Grassineau, N., Guido, D.M., 2015. Archean (3.33 Ga) microbe-sediment systems were diverse and flourished in a hydrothermal context. *Geology* 43, 615–618. <https://doi.org/10.1130/G36646.1>

Figure captions

Figure 1. A- Simplified geological map of the Anti-atlas of Morocco. B- Structural Map of Oued Dar'a caldera showing the localization of the studied area (Chraiki et al., 2020).

Carte géologique simplifiée de l'Anti-atlas du Maroc. B- Carte structurale de la caldeira de Oued Dar'a montrant la localisation de la zone étudiée (Chraiki et al., 2020).

Figure 2. Detailed lithostratigraphic column of the Amane Tazgart succession (modified from (Chraiki et al., 2020)

Colonne lithostratigraphique détaillée de la succession d'Amane Tazgart (modifié de (Chraiki et al., 2020)

Figure 3. Structures and diversity of carbonate microbialites from the lower part of Amane section: A- Thrombolitic coalescent domes. B- General view of large domal stromatolites and coalescent domes of composite microbialites. C- Thrombolites dominated by patchy carbonate mesoclotls surrounded by cement or fine-grained epiclastic matrix. D- Composite microbialitic dome showing the occurrence of laminated (Lm) and clotted (Cl) fabric together in the same dome. E- Laterally linked flat large domal stromatolites. F- Columnar and domal carbonate stromatolites. G- Section view across polygonal stromatolites showing upturned margins H- View from the surface of polygonal stromatolites showing two networks of upturned margins.

Structures et diversité des microbialites carbonatées de la partie inférieure de la section d'Amane : A- Dômes thrombolitiques coalescents. B- Vue générale de grands stromatolites domaux et de dômes coalescents de microbialites composites. C- Thrombolites dominées par des mésoclotls carbonatés épars entourés de ciment ou d'une matrice épiclastique à grain fin. D- Dôme microbialitique composite montrant l'occurrence de tissu laminé (Lm) et coagulé (Cl) ensemble dans le même dôme. E- Stromatolites plats et larges en forme de dôme, reliés latéralement. F- Stromatolites carbonatés en colonne et en dôme. G- Vue en coupe de stromatolites polygonaux montrant des marges retournées H- Vue de la surface de stromatolites polygonaux montrant deux réseaux de marges retournées.

Figure 4. Vertical evolution of the fabric showing the transition from clotted-dominated to laminated-dominated microbialites. A- Thin section from a thrombolite (Ms: mesoclotls). B-

Thin section of composite microbialite showing the dominance of clotted fabrics associated with laminated fabrics (yellow arrow) at the mesoscale (Ms: mesoclots). C- Thin section of large domal stromatolites showing the typical textures of tufted microbial mats (yellow arrows). D- Thin section of composite microbialite showing the dominance of laminated fabric (LMs: laminated mesoclots, Ms. mesoclots). E- Thin section of the last stromatolitic facies of carbonate succession. F- Thin section of planar to pseudo-columnar epiclastic stromatolites. G- Thin section of columnar epiclastic stromatolites. H- Thin section of conical stromatolites. I- Thin section of domal stromatolites.

Evolution verticale de la mésostructure des microbialites montrant la transition entre les microbialites à dominance coagulée et celles à dominance laminée. A- Microfaciès d'une thrombolite (Ms : mésoclots). B- Microfaciès d'une microbialite composite montrant la dominance des fabriques coagulés associés à des fabriques laminés (flèche jaune) à la mésos-échelle (Ms : mesoclots). C- Microfaciès des stromatolites en dome larges montrant les textures typiques des tapis microbiens touffus (flèches jaunes). D- Microfaciès de microbialite composite montrant la dominance des structures laminés (LMs : mésoclots laminés, Ms : mésoclots). E- Microfaciès du dernier faciès stromatolitique de la succession carbonatée. F- Microfaciès des stromatolites épilastiques horizontaux à pseudo-columnaires. G- Microfaciès de stromatolites épilastiques columnaires. H- Microfaciès de stromatolites en cones. I- Microfaciès de stromatolites en dôme.

Figure 5. Field view and drawing of the last microbialitic bed of Amane Tazgart, showing the morphotypes diversity from bottom to top.

Vue générale et reconstruction du dernier niveau microbialitique d'Amane Tazgart, montrant la diversité des morphotypes du bas en haut.

Figure 6. A- Diversity and structures within the clastic microbialitic bed: A- Planar wrinkly laminated to pseudo-columnar stromatolites from the bottom followed by columnar stromatolites. B-C Views from section and bed surface of laterally linked columnar-hemispherical stromatolites. D- View of two-bed surfaces illustrating the transition from columnar to domal morphotypes. E- Section across typical large stromatolitic dome. F- Cone-shaped linked domes. G- Large composite dome between which are several small-scale domes (yellow arrow). H- Large composite dome (1) separated by interdome epiclastic deposits (3)

showing an alternation of continuous stromatolitic layers (2, 4). I- Vertical cross-section view of interdome deposits showing the alternation of stromatolitic and clastic layers.

A- Diversité et structures des microbialitiques clastiques : A- Stromatolites horizontaux laminés et ondulés à pseudo-columnaires du bas en haut suivis par des stromatolites columnaires. B-C Vues de la section et de la surface du niveau de stromatolites columnaires-hémisphériques liés latéralement. D- Vue de deux surfaces de lits illustrant la transition entre les morphotypes columnaire et en dôme. E- Coupe à travers un grand dôme stromatolitique. F- Dômes liés en forme de cône. G- Large dôme composite au sein duquel se trouvent plusieurs dômes de petite taille (flèche jaune). H- Grand dôme composite (1) séparé par des dépôts épiclastiques d'interdômes (3) montrant une alternance de couches stromatolitiques continues (2, 4). I- Vue en coupe verticale des dépôts d'interdômes montrant l'alternance de couches stromatolitiques et clastiques.

Figure 7. A- Thin-section photomicrograph of thrombolites showing mesoclot within a matrix preserving wavy and wrinkly dark crusts (Ms= mesoclot, CF= calcite fans, LMt= laminated matrix). B- Thin section photomicrograph showing a core of a mesoclot (delimited with yellow dashed ligne) surrounded by an outer layer of fibrous calcite. The voids of this case are composed of drusy calcite that was replaced locally by silica (red arrow) (DC= Drusy calcite, Si= silica). C- Thin-section photomicrograph of thrombolites with laminated clots surrounded by drusy calcite. D- Thin section photomicrograph of a composite microbialite illustrating the association of clotted (Ms) and laminated fabrics (red arrows). E- Thin-section photomicrograph of flat large domal stromatolites consisting of tufted microbial iron crusts (yellow arrows), alternating with dark micritic to microsparitic laminae (Ir= Iron crust, Sp= micritic to microsparitic laminae). F- Thin-section photomicrograph of carbonate stromatolite (Mi= micritic laminae, Gl= grain-sized laminae). G- Thin-section photomicrograph of flat laminated clastic stromatolites. H- Thin-section photomicrograph of columnar stromatolite illustrating the presence of gas escape structures (delimited by a yellow dashed line). I- Thin-section photomicrograph of domal stromatolites composed of tufted grain-sized microbial mats (Gl) and sparry crust (Sp) (Pl= flattened peloids, Tf= tufts). J- Thin-section photomicrograph illustrating the opaque color of micritic laminae under cross-polarized light (Sp= Sparry crust, Mi= micritic laminae). K- Photomicrograph of a clastic stromatolite showing an iron-rich (Ir) micritic laminae alternated with microsparitic laminae (Tf=Tuft). L- Thin-section photomicrograph of flat laminated to pseudocolumnar stromatolites of the interdome space. This microfabric consists of an alternation of coarse-grained wrinkled

laminae and wrinkled iron-rich laminae (Ic) bounding isolated silt and sand-sized clastic grains (yellow arrow).

A- Microfaciès de thrombolites montrant des mésoclots dans une matrice préservant des croûtes sombres ondulées (Ms = mésoclot, CF = éventails de calcite, LMt = matrice laminée). B- Microfaciès montrant un noyau de mésoclots (délimité par une ligne pointillée jaune) entouré d'une couche externe de calcite fibreuse. Les vides sont composés de calcite drusique qui a été remplacée localement par de la silice (flèche rouge) (DC = calcite drusique, Si = silice). C- Microfaciès de thrombolites avec des mésoclots laminés entourés de calcite drusique. D- Microfaciès d'une microbialite composite illustrant l'association de fabriques coagulés (Ms) et laminés (flèches rouges). E- Microfaciès de stromatolites plats et larges, constitués de croûtes de fer microbiennes en pinnacles (flèches jaunes), alternant avec des lames sombres micritiques à microsparitiques (Ir = croûte de fer, Sp = lames micritiques à microsparitiques). F- Microfaciès d'un stromatolite carbonaté (Mi = lames micritiques, Gl = lames granuleuses). G- Microfaciès de stromatolites clastiques laminés plats. H- Microfaciès d'un stromatolite columnaire illustrant la présence de structures d'échappement de gaz (délimitées par une ligne pointillée jaune). I- Microfaciès d'un stromatolite en dome composé d'un tapis microbien de la taille d'un grain (Gl) et d'une croûte spartique (Sp) (Pl = péloïdes aplatis, Tf = pinnacle). J- Microfaciès illustrant la couleur opaque des lames micritiques sous lumière polarisée analysée (Sp = croûte sparifique, Mi = lames micritiques). K- Microfaciès d'un stromatolite clastique montrant des lames micritiques riches en fer (Ir) alternant avec des lames microsparitiques (Tf =pinnacle). L- Microfaciès de stromatolites plats laminés à pseudo-columnaires de l'espace d'interdome. Cette microfabrique consiste en une alternance de lames ondulées à gros grains et de lames ondulées riches en fer (Ic) délimitant des grains clastiques isolés de la taille d'un silt ou d'un sable (flèche jaune).

Figure 8. A- Thin section photomicrograph of a clastic stromatolite showing a hematite coarse-grained wrinkled laminae. B- Raman spectra of the red point in Fig. (8A). C- Thin section photomicrograph of clastic stromatolite showing dark micritic laminae. D- Raman spectra of the red point in Fig. (8C) (Red circle: Point of the Raman analysis).

A- Microfaciès de stromatolites clastiques montrant des lames d'hématites à gros grains. B- Spectre Raman du point rouge de la figure (8A). C- Microfaciès de stromatolites clastiques

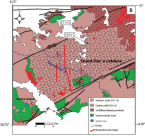
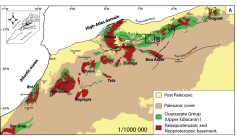
montrant des lamination micritiques sombres. D- Spectre Raman du point rouge de la Fig. (8C) (cercle rouge : point de l'analyse Raman).

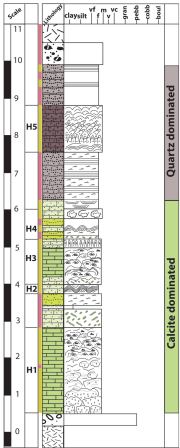
Figure 9. A) Upper bedding surface showing densely packed stromatoclastes with various shape and size, B) Sandy limestone with cross laminations showing symmetrical profils (coin is 2.4 cm in diameter), C) Thinly bedded sandstone with bedding surface showing small-scale symmetrical ripples with winding and bifurcation of crests (pen is 14 cm long) D) Bedding surface of fine grained sandstone showing asymmetrical ripples with bifurcating crests (coin is 2.5 cm in diameter).

A) Surface du litage supérieur montrant des stromatoclastes densément tassés de forme et de taille variées, B) Calcaire gréseux avec des lamination croisées montrant des profils symétriques (pièce de 2,4 cm de diamètre), C) Grès à lit mince avec une surface de litage montrant des ondulations symétriques à petite échelle avec un enroulement et une bifurcation des crêtes (stylo de 14 cm de long) D) Surface du litage du grès à grain fin montrant des ondulations asymétriques avec des crêtes bifurquées (pièce de 2,5 cm de diamètre).

Figure 10. Schematic depositional model for microbial deposits in Amane Tazgart highlighting the distribution, characteristics, and morphologies of biogenic and abiogenic deposits in carbonates (A) and epiclastic deposits (B).

Modèle schématique de dépôt des accumulations microbiennes d'Amane Tazgart mettant en évidence la distribution, les caractéristiques et les morphologies des dépôts biogènes et abiogènes dans les faciès carbonatés (A) et les faciès épiclastiques (B).





Legende

Lithology

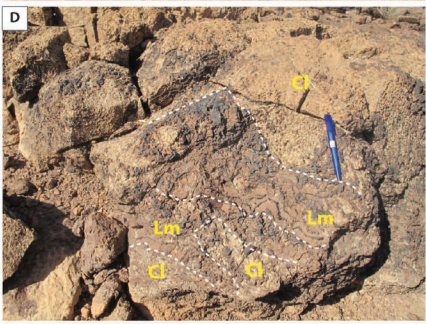
- Carbonate
- Sandy limestones
- Calcarenite
- Sandstones
- Clastic stromatolites
- Silty sands
- Conglomerates
- Peperites
- Andesites

Sedimentary structures

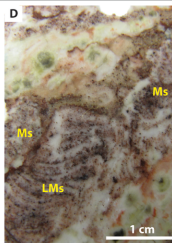
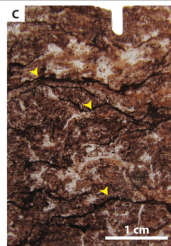
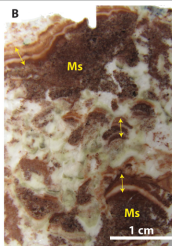
- Microbialite-derived clasts
- Ripple cross lamination
- Planar lamination
- Composite microbialites
- Polygonal stromatolites
- Domal microbialites
- Flat domal stromatolites
- Columnar stromatolites
- Spherulites
- Thrombolites

Facies type

- Microbial origin
- Physical origin



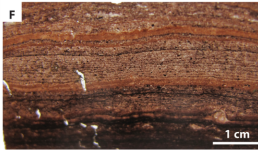
Carbonate microbialites



Clotted fabric

Laminated fabric

Epiclastic microbialites



100 % Laminated fabric



Planar



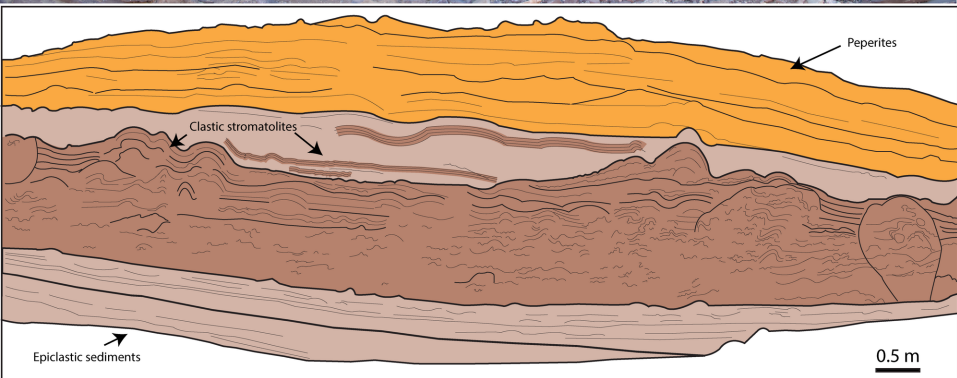
Columnar



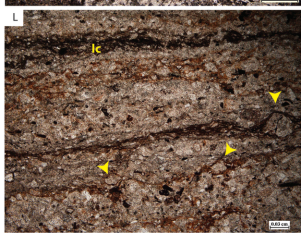
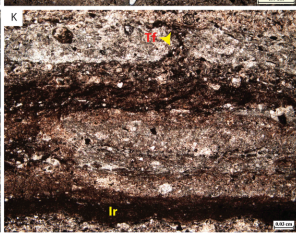
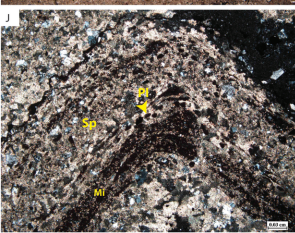
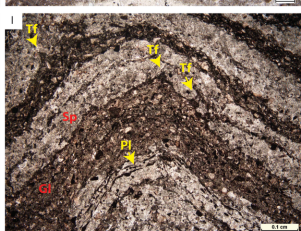
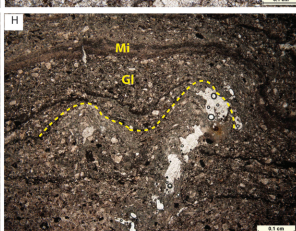
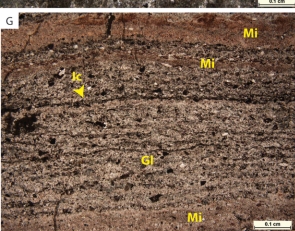
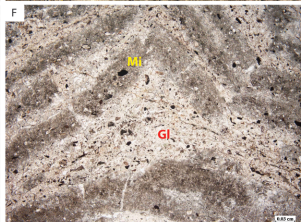
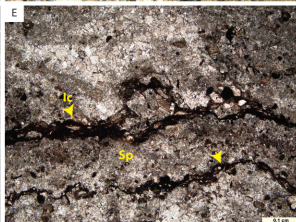
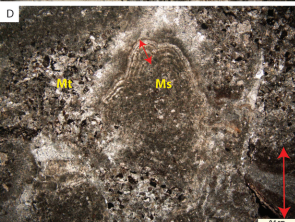
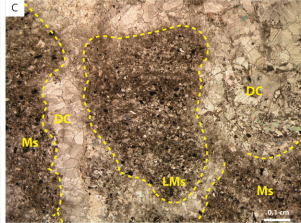
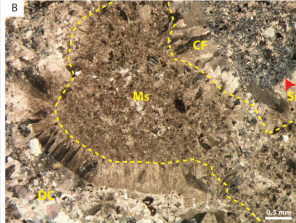
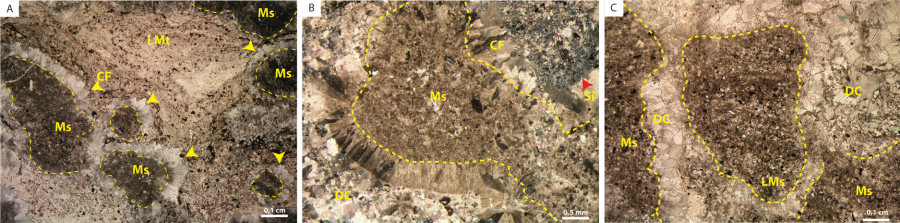
Conical

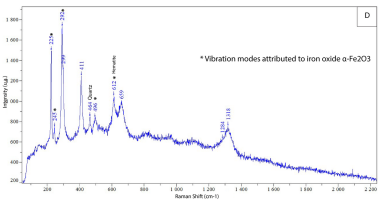
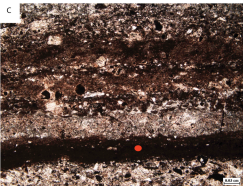
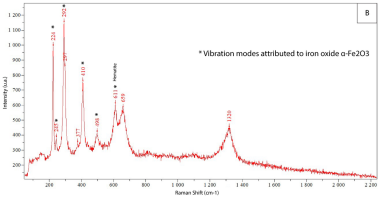
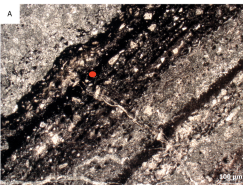


Domal









A



B



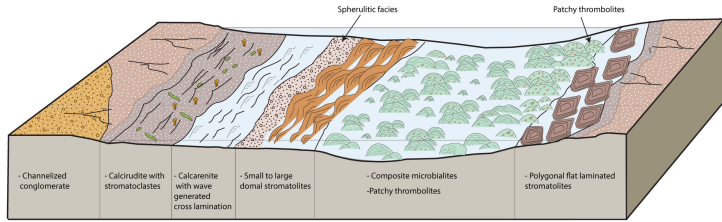
C



D



A



B

